Contents

List of Figures

Force and Pressure Distribution in Polydisperse Packing of Spheres in 2 and 3 Dimensions

Anthony Bourached

March 16, 2015

Abstract

We report on the analysis of data created by contact dynamic simulations to determine the functional form of the distribution of normal forces and normal pressures found in 2- and 3- dimensional random packings of granular media under uniaxial compression, as well as the effect of the degree of polydispersity on the force distribution. We observe that in 2D: the functional form of the tail of the force distribution is very close to an exponetial and gets gets rapidly closer as polydispersity increases. It is also found that greater polydispersity increases the standard deviation of the force distibution. The functional form of the pressure distribution's tail is a gaussian and can be fit to form axe^{bx^2}. We observe that in 3D: the function form of the tail for force and pressure is a streched exponential (ae^{bx^α}) with $\alpha = 0.58$ for force and $\alpha = 1.58$ for pressure.

1 Introduction

The most basic example of granular materials that can be considered is a static assembly of spherical particles in contact and placed under uniaxial compression. We call this configuration a packing. The system is under stress from the compressing force and so most of the particles in this packing will experience forces between itself and other spheres with which it is in contact. A small portion do not experience any force and hence are not constrained and are free to move within a space. We refer to these particles as rattlers. Since the packing is in equilibrium, the sum of the forces on each particle must equal zero. Even in this ideal case, the distribution of the forces in the packing is complicated to predict.

A monodisperse packing of particles in 2-dimensions will result in a crystalline structure and might imply a homogeneous force distribution (uniform load sharing amongst the grains). But this assortment of perfect particles is clearly only a hypothetical situation and the slightest variation in size or shape of the particles, which will be present in any practical situation, as well as the way in which they are packed, shall result in an inhomogeneous distribution of force. This causes stresses to be transmitted throughout the packing via force chains which

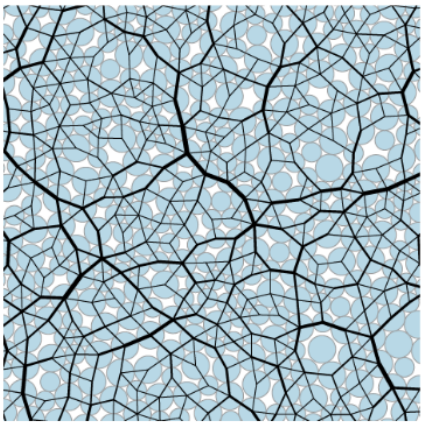

Figure 1: Force Chains in a 2 dimensional packing of spheres [2]

makes up a network of grains that share most of the stress from the applied load amongst a small fraction of the overall grains [4]. An image of force chains in a two dimensional packing is shown in figure 1.

Spatially inhomogeneous distribution of force and pressure amongst grains in a packing is characteristic of granular media. Many 2D and 3D experiments have produced a prediction of a functional form of the force and pressure distribution in polydisperse packings. Paper by P. Tighe et al [3] used an entropy maximising procedure to derive an analytical solution for the normal probability distribution of pressure in monodisperse, 2D packings:

$$\rho(p) = Z^{-1} p^{\nu} \exp(-\alpha p - \gamma \langle a(p) \rangle) \tag{1}$$

They show that for a frictionless system, the term $\langle a(p) \rangle$ is quadratic and so the exponential term is gaussian. In the region of $p > \bar{p}$ the exponential term in (1) becomes dominant and so the function becomes gaussian in that region. It is said in this case that the distribution has a gaussian tail. It is also possible to see that in the region $p < \bar{p}$ the dominant term is p^{ν} and so is characterised by a power law in this region. Tighe et al also makes a prediction that in 3D monodisperse packings the functional form of the tail is; $\rho(p) \sim \ e^{-p^{\delta}}$ where $\delta = 3/2$ while noting that numerical solutions have found it to be $\delta \approx 1.7 \pm 0.1$ This is the form of a stretched exponential.

In paper Mueth et al. [4], the functional form of a 3D monodisperse packing was found experimentally by measuring the force exerted on each constraining surface of the container, in which the granular material was held, using a carbon paper technique [4]. This functional form of the force distribution, in contrast to the functional form of the pressure distribution, found by other numerics as mentioned in Tighe et al. [3] as well as their own analytical extrapolations was also found to have a tail of the form of a stretched exponetial ($e^{-p^{\delta}}$) where δ was found to be in the range $1.0 < \delta < 1.9$, depending on the coefficient of friction for the system, and to have a nearly uniform distribution below the mean force. The functional form of the force distribution in 2D, however, has been found by experimental simulations

in paper by Radjai et al. [5] to have an exponential decay $\rho(f) \sim \ e^{-f^{\delta}}$ in the region $p > \bar{p}$ with $\delta = 1$ rather than a gaussian ($\delta = 2$), as is the case for 2D pressure distribution [3], while in the region $p < \bar{p}$, the dominant term is found to obey a power law $\rho(f) \sim \ f^{\nu}$.

2 Motivation and Aims

While many papers have revealed both analytical and experimental results which generally agree it is possible to see shortcomings in some of the methods. Ideally, both numerical and analytical agreement is required to accept a model. In lab orientated experiments like Mueth et al. [4] it is impractial to determine the repulsive force between contacts. Instead only forces due to contact with the containing surfaces are possible to calculate. Thus the pressure distribution is impossible to determine by this method and so we must find an alternative way to see if numerics agree with the analytical solutions presented by Tighe et al. [3].

It is also notable that the effect of polydispersity on the functional form can not be accurately determined in a lab orientated experiment as it is impractical to prepare a packing of grains with gaussian distributed radii. It is the aim, therefore, of this paper to present a numerical prediction of the functional form of the force and pressure distribution by analysing contact dynamic simulations thereby making it possible to accurately determine pressures and contact numbers, as well as enabling us to produce an ideal set of spheres of desired dispersity. With many such packings we believe we can make accurate predictions of the functional form of both pressure and force distribution and also determine the the effect that polydispersity has on the force distribution, which, for the reasons above, has not been explicitly tested before.

3 Methodology

In this paper we analysed data prepared by Cathal B. O'Donovan [2] in which packings were simulated using two methods: The Bubble Mode Code and the Conjugate Gradient Minimisation. The Bubble Mode Code protocol in 2D created 1500 discs (soft bubbles) in a periodic box, with dimensions of unit 1, initially at a very low packing fraction ϕ. Periodic boundary conditions were used. Their radii were slowly increased until a desired packing fraction Φ was reached. There is no distortion of shape when an interaction between bubbles occurs but instead a simple overlap in space is allowed, with energy created by the extent of overlap between bubbles. The bubles are allowed to move freely, tending to minimise the energy due to overlap, and the simulation was terminated when the energy reached a steady state minimum. Several packings are made with several different packing fractions for different gaussian polydispersities. Several data files were made containing the position, in cartesian coordinates, and radii of each sphere.

We analysed five data sets:

1. 2 Dimensional:
   (a) Bi Dispersive; (bi) Standard Deviation $\approx 0.17\ \bar{r}$
   (b) Polydispersive; (g29) with a gaussian distribution of radii Standard Deviation $\approx 0.29\ \bar{r}$
   (c) Polydispersive; (g25) with a gaussian distribution of radii Standard Deviation $\approx 0.25\ \bar{r}$
   (d) Polydispersive; (g14) with a gaussian distribution of radii Standard Deviation $\approx 0.14\ \bar{r}$
2. 3 Dimensional:
   (a) Monodispersive

Each 2D data set had 50 packings with approximately 15,000 spheres per packing, while the 3D data set had 500 packings. Since we are dealing with a probability distribution a very large number of data points were required to yield a decent prediction of the distribution. This is especially important for the tail, as in all cases there seems to be a severe drop-off of the probability density meaning that the tail contains fewer data points.

We wrote a script in Python to determine the force and pressure distribution from all the packings in a given data set. The force between two contacts was determined using Hooke's law by calculating the overlap δ, as seen in figure 2.

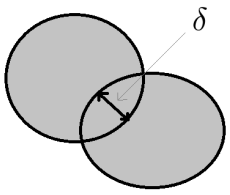

Figure 2: Overlap between spheres gives contact force by hooke's law $F = -\delta k$.

The pressure for each sphere, i, could then be found by summing over its contact forces and dividing by its surface area

$$P_i = \frac{\sum_j F}{Surface\ Area_i}$$

The data was non-dimensionalised and placed in bins of appropriate size to have a reduced level of noise while having as many bins as possible. Bin size was increased where there was a surplus of data points, making the shape graph easier to distinguish, and reduced in any regions where a lesser amount of data points were analysed. Boundary conditions were also taken into consideration. The code was elaborated for the 3D packings to account for the extra cartesian coordinate and the boundary conditions were also modified appropriately. The particles were assumed to be massless for all parts. The code was ran once for each data group and the results were recorded for analysis.

4 Results and Analysis

4.1 2D

Figure 3 shows an overplot of the force distribution and pressure distribution from the created data. We can see in both cases that the peak is to the left of the mean force or pressure, i.e. most of the grains experience a below average amount of force or pressure. It was also found that 5-6% of spheres were rattlers (experiencing no force or pressure). From figure 3b, we see that some spheres experience at least 4 times more pressure than the average. These observations support the force chain model given in jounral by Tighe et al. [1] as seen in figure 1 and confirms that most of the stresses are experienced by a minority of grains.

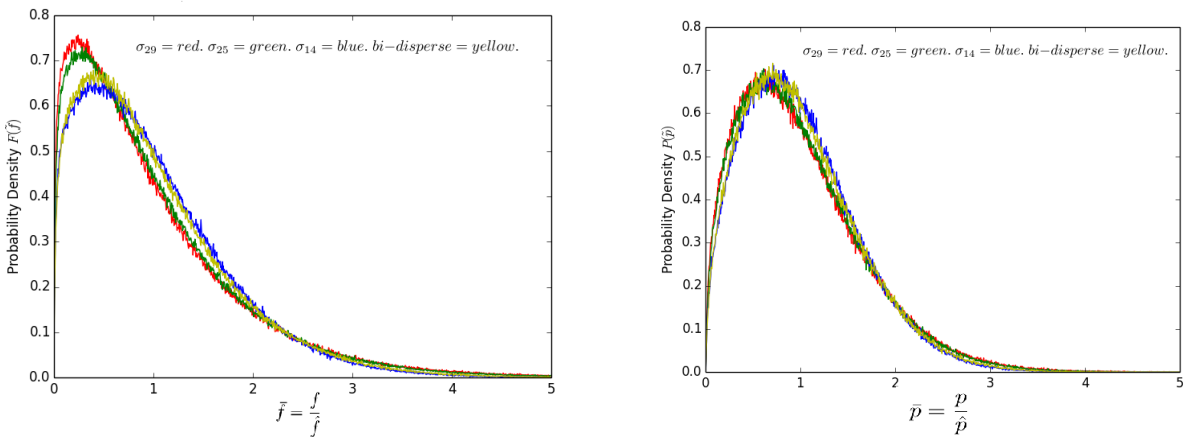

(a) Force density distributions.

(b) Pressure density distributions.

Figure 3: Force and pressure densities distributions. Bin size 0.005

To determine the force and pressure distributions we predominantly consider the functional form of the distributions in regions: $f > \bar{f}$ for the force and $p > \bar{p}$ for the pressure, which can be referred to as the tail.

4.1.1 Force

Linear semilog plots, as seen in figures 4 and 5 verify an exponential functional form for the force distribution in the region $f > \bar{f}$. A line was fitted to semilog plots of each data set, with a trend of better fit for higher standard deviations. This may be seen by looking at the extremes of the data, as seen in figure 5. Fits to all the data sets, with larger bin sizes can be seen in figure 11 found in the appendix.

This does not necessarily imply that ploydispersity affects the functional form of force distribution, since, if we consider figure 3a, we see that the peak for packings with higher standard deviations are further from the mean. This implies that the force distribution is more spread.

This can also be seen from figure 12, found in the appendix.

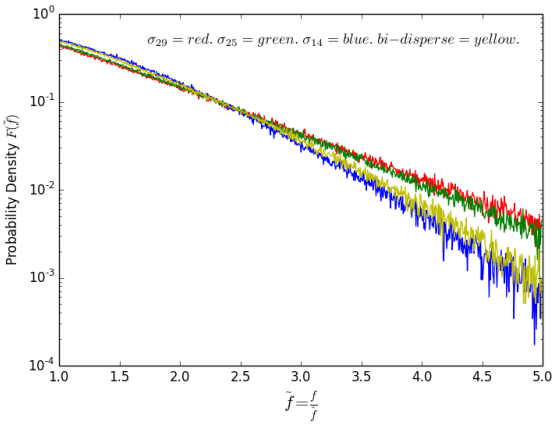

Figure 4: Overplot of the log of the force distribution vs. the force. All four data sets are shown here. Bin size 0.005

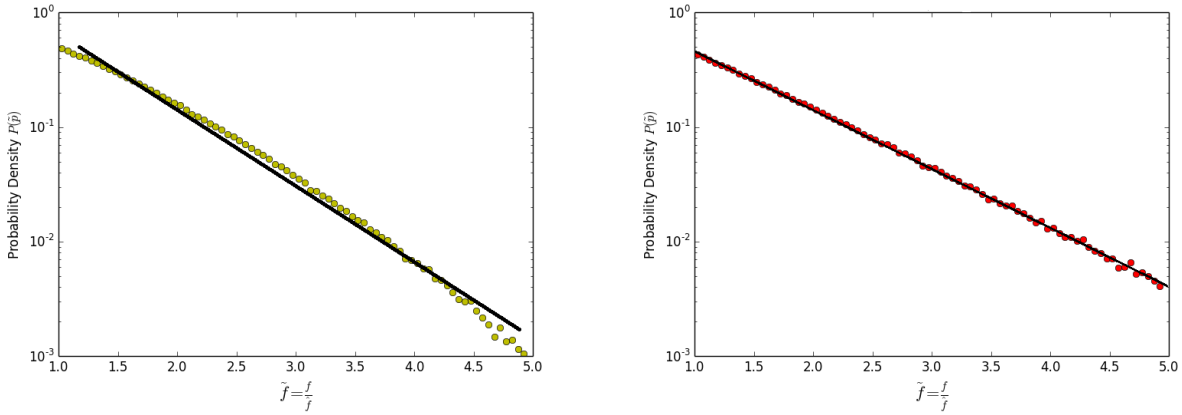

(a) Linear fit to semilog of g14 data.

(b) Linear fit to semilog of g29 data.

Figure 5: The extremes of data, plotted as $\log(\rho(f))$ Vs. f, g29 has the highest standard deviation of all the 2D data and g14 has the lowest. The bin size for these plots was set to 0.05.

A more diverse force distribution may imply that the shape is more representative of the correct form, especially for the tail where there will be fewer data points for a less spread distribution. However, we can see from figure 3a that in the region between $1\hat{f}$ and $2\hat{f}$, g14 should have a slightly higher number of data points than g29 due to its higher probability density in this region. So it would be expected that figure 6a would have a linear fit which

is in as strong an agreement as figure 6b, but we can see that this is not the case and that g29 still has a substantially better fit. This means that it is not the wider distribution of data that causes a better linear fit with greater polydispersity, but that as polydispersity increases, the functional form of the force distribution very rapidly approaches an exponential.

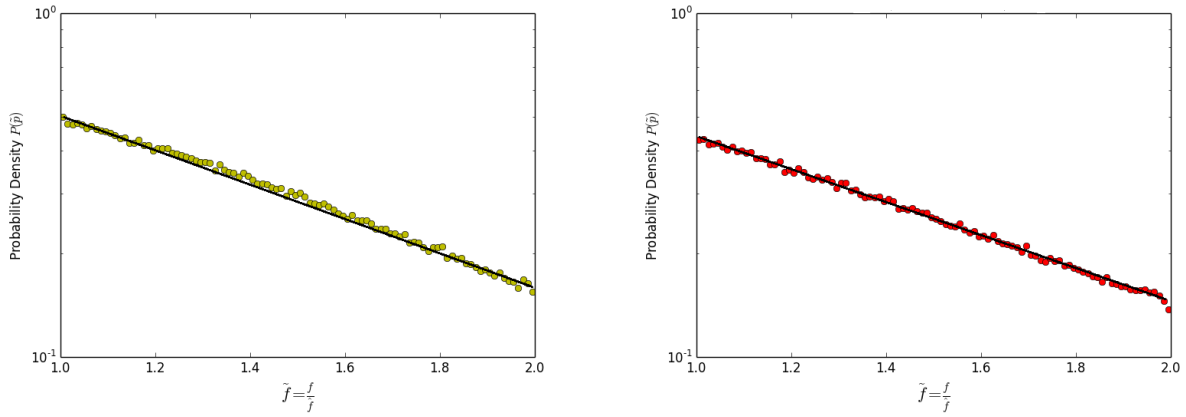

(a) Linear fit to semilog of g14 data.

(b) Linear fit to semilog of g29 data.

Figure 6: The extremes of data plotted in the range $1\hat{f}$ and $2\hat{f}$ plotted as $\log(\rho(f))$ Vs. f. Bin size = 0.05

4.1.2 Pressure

Linear plots of the log of the pressure distribution vs. pressure squared, as seen in figure 7, and figures 13 and 14 found in the appendix verify a gaussian functional form in the region $p > \bar{p}$.

All data sets had good linear fits. Slightly better fits are observed for lower polydispersities, as can be seen from the extremes of the data in figure 7.

It appears that polydispersity has a less significant effect on the functional form of the pressure distribution than it does on that of the force distribution. However, the results in figures 7 and 14 suggest that the functional form diverges, very slowly, from a gaussian with increasing polydispersity. A function that has a gaussian term that dominates in the region $p > \hat{p}$ can be fitted to the data as shown in figure 8.

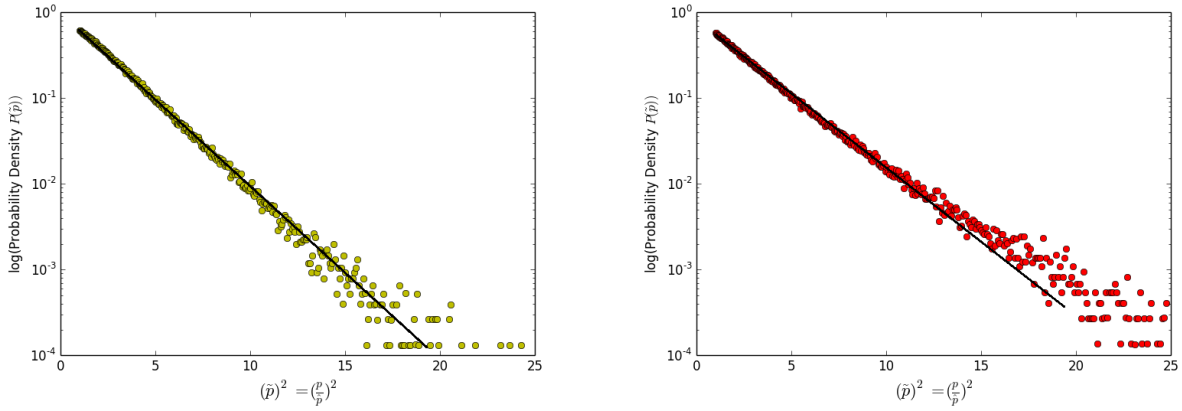

(a) Linear fit to semilog of g14 data pressure.

(b) Linear fit to semilog of g29 data pressure.

Figure 7: The extremes of data, plotted as $\log(\rho(p))$ Vs p^2. Bin size = 0.01

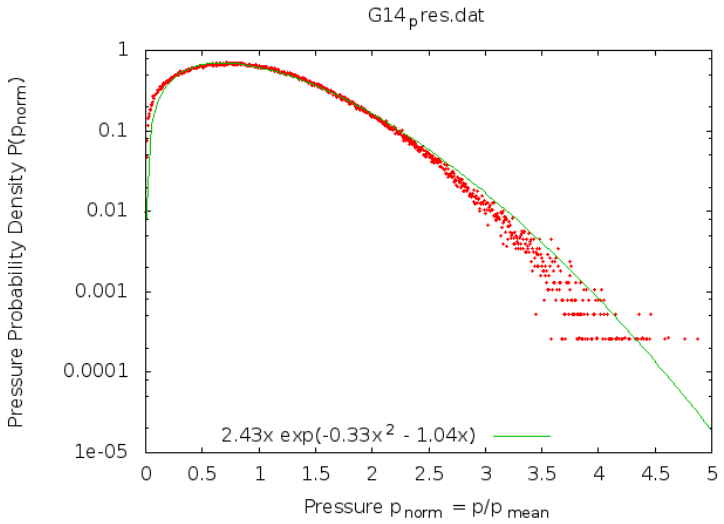

Figure 8: Functional fit to g14 pressure distribution.

The exponent is quadratic, which is equivalent to a shifted gaussian. The x term will be dominant in the region $p < \hat{p}$. This is a power law with degree 1 and is of the form predicted by Tighe et al [3] and by Radjai et al. [5]. Functional fits to all the data may be seen in figure 15, found in the appendix.

4.2 3D

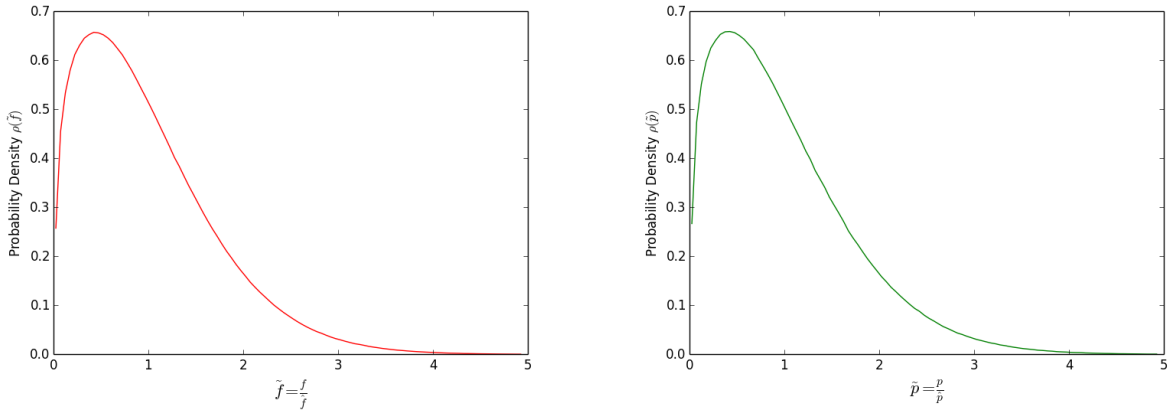

(a) Force (b) Pressure

Figure 9: Probability distributions of force and pressure. Bin size = 0.05

Figure 9 shows the probability distribution for force and pressure for the 3D data set. A linear fit to the tail of the log of the log of the probability distribution vs. log of the force and of the pressure verifies a function form of a stretched exponential $f(x) = ae^{-bx^{\alpha}}$, as seen in figure 10 for the force and pressure distributions. It is of particlular interest to note that $\alpha_p \approx \alpha_f + 1$ as is also the case in 2D.

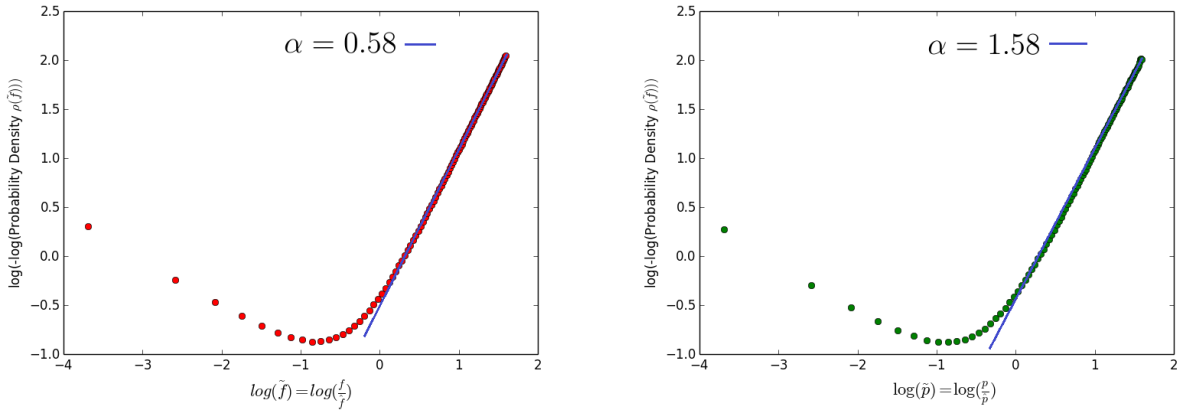

(a) Force (b) Pressure

Figure 10: log of the log of probability distribution vs. log of the force/pressure. Bin size = 0.05

5 Conclusion

In 2D, the tail of the force distribution is characterised by a functional form that very rapidly approaches an exponential with increasing polydispersity. A highly polydispersive packing results in a a very good exponential fit. Greater polydispersities increases the standard deviation of the force. It was found that the functional form of the tail of the pressure distribution is gaussian in agreement with analytical prediction by Tighe et al. [3]. This gives better fit for low polydispersities, therefore the function form of the tail approaches gaussian for decreasing polydispersity. Using this information it was possible to make a fit of the functional form, given by Tighe et al. [3], to the distribution. In 3D, the functional form of the force and pressure distribution is a stretched exponential ($f(x) = ae^{-bx^{\alpha}}$), with $\alpha = 0.58$ for force distribution and $\alpha = 1.58$ for pressure distribution. It is of particular interest to note that, similar to the 2D case, $\alpha_p \approx \alpha_f + 1$. Analysis of more data sets with both larger and smaller polydispersities would be required to more accurately determine the effect of polydispersity on the functional form of the force and pressure distributions in 2D, and would be the most natural continutation to this work.

6 Acknowledgements

I'd like to thank Prof. Matthias Möbius, for his guidence and many useful conversations. I also thank my partner in this project, Kevin Mooney.

References

[1] Brian P. Tighe[1] and Thijs J. H. Vlugt[2], Force balance in canonical ensembles of static granular packings, Journal of Statistical Mechanics: Theory and Experiment (2010)

[2] Cathal B. O'Donovan, The Structure and Flow of Disordered Wet Foams, Thesis, School of Physics, Trinity College Dublin (2013)

[3] Brian P. Tighe[1], Adrianne R. T. van Eerd[2], and Thijs J. H. Vlugt[3], Entropy Maximization in the Force Network Ensemble for Granular Solids, Physics Review Letters (2008)

[4] Daniel M. Mueth, Heinrich M. Jaeger, Sidney R. Nagel, Force Distribution in Granular Medium, The James Franck Insitute and Department of Physics, University of Chicago, 5640 Ellis Ave., Chicago, IL 60637

[5] Farhang Radjai, Michel Jean, Jean-Jacques Moreau, and Stphane Roux, Force Distributions in Dense Two-Dimensional Granular Systems, Phys. Rev. Lett. 77, 274 (1996)

Appendix

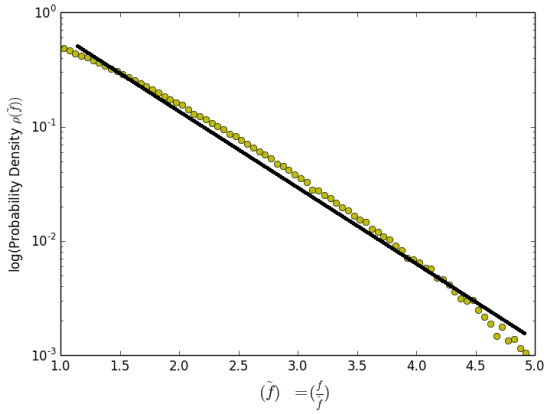

(a) Bi dispersive.

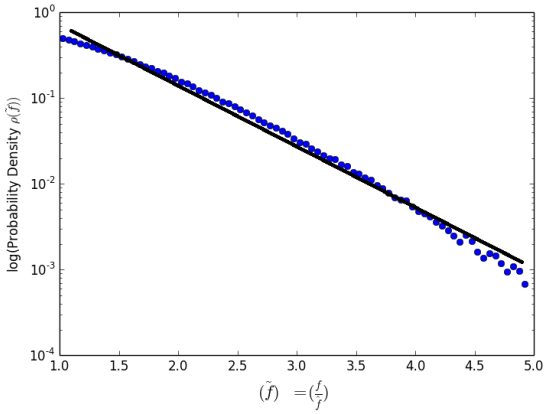

(b) g14

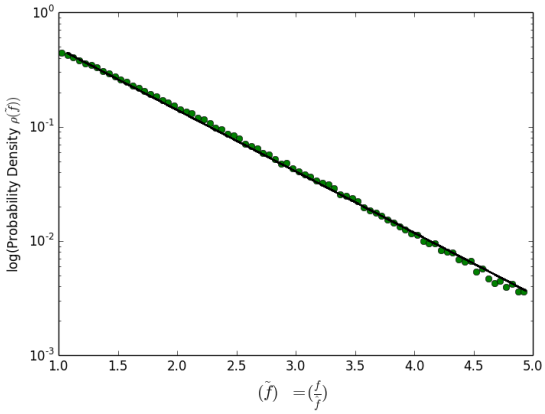

(c) g25

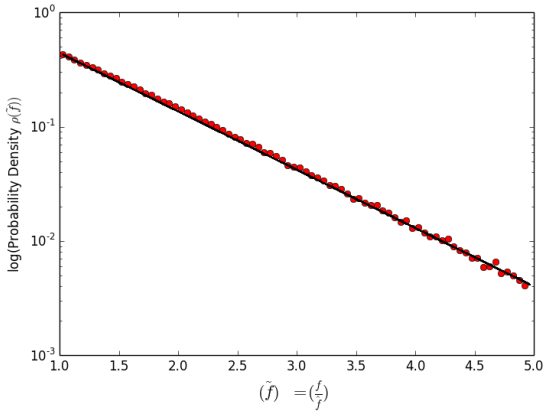

(d) g29

Figure 11: Log of the force distribution vs. force. Bin size = 0.05

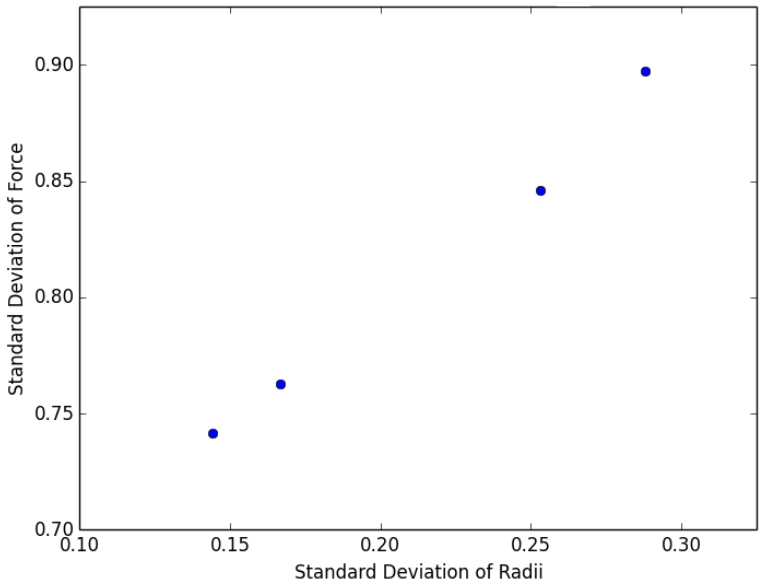

Figure 12: Affect of Standard Deviation of radii on Standard Deviation of Force

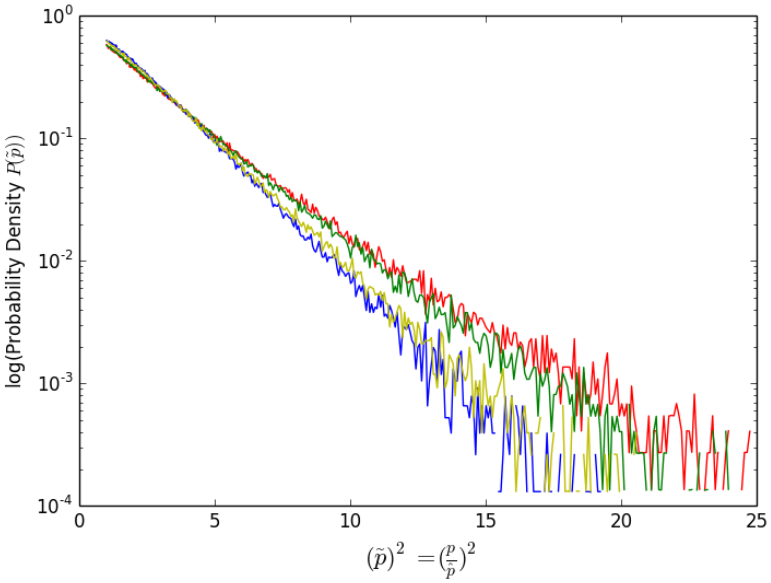

Figure 13: Overplot of the log of the probability distribution vs. the pressure squared. Bin size = 0.01

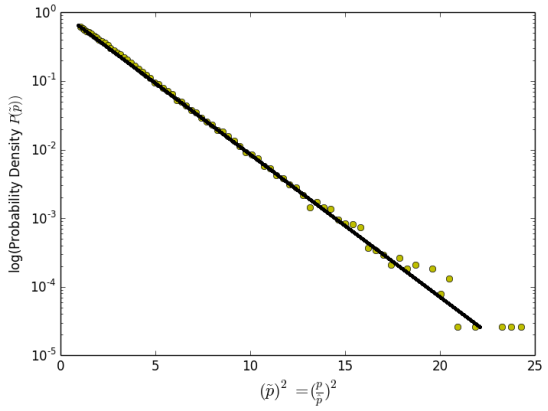

(a) Bi dispersive.

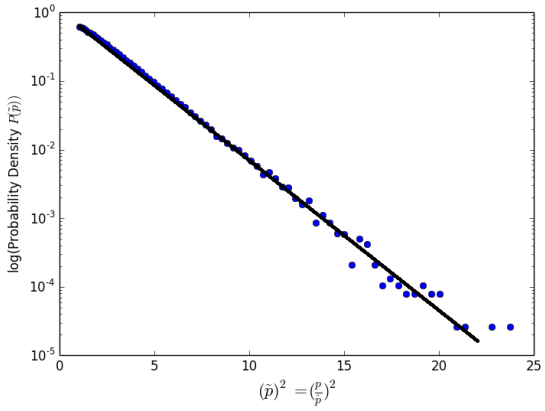

(b) g14

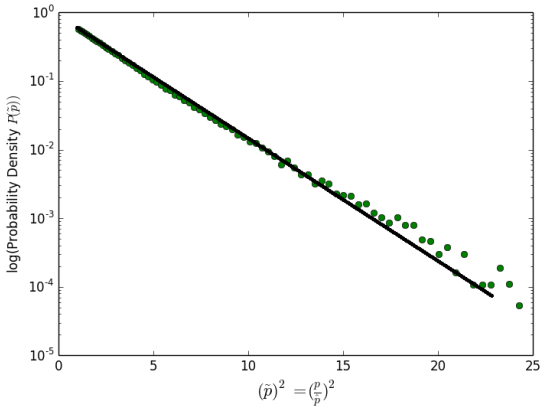

(c) g25

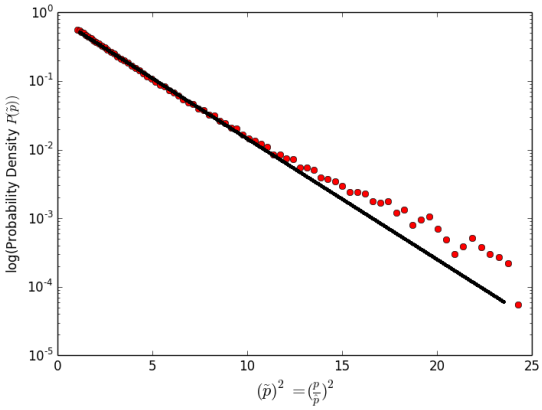

(d) g29

Figure 14: Log of the pressure distribution vs. pressure squared. Bin size = 0.05

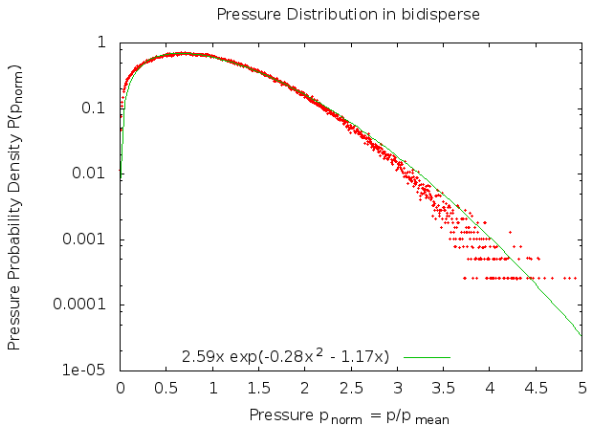

(a) Bi dispersive.

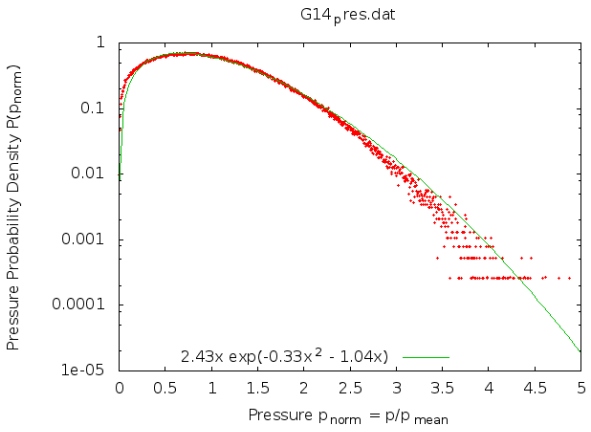

(b) g14

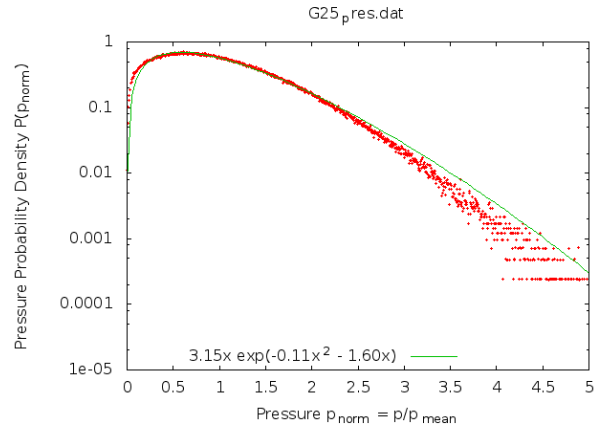

(c) g25

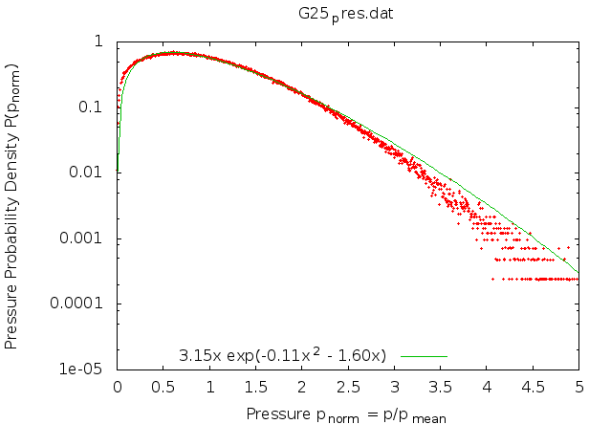

(d) g29

Figure 15: Function fit to pressure distributions.